NEOPLASIA
www.neoplasia.com

Volume 20 Number 10 October 2018 pp. 1008–1022 1008

AXL Mediates Esophageal Adenocarcinoma Cell Invasion through Regulation of Extracellular Acidification and Lysosome Trafficking[1]

Selma Maacha[*], Jun Hong[*], Ariana von Lersner[†], Andries Zijlstra[†] and Abbes Belkhiri[*]

[*]Department of Surgery, Vanderbilt University Medical Center, Nashville, TN 37232, USA; [†]Department of Pathology, Microbiology, and Immunology, Vanderbilt University, Nashville, TN 37240, USA

Abstract

Esophageal adenocarcinoma (EAC) is a highly aggressive malignancy that is characterized by resistance to chemotherapy and a poor clinical outcome. The overexpression of the receptor tyrosine kinase AXL is frequently associated with unfavorable prognosis in EAC. Although it is well documented that AXL mediates cancer cell invasion as a downstream effector of epithelial-to-mesenchymal transition, the precise molecular mechanism underlying this process is not completely understood. Herein, we demonstrate for the first time that AXL mediates cell invasion through the regulation of lysosomes peripheral distribution and cathepsin B secretion in EAC cell lines. Furthermore, we show that AXL-dependent peripheral distribution of lysosomes and cell invasion are mediated by extracellular acidification, which is potentiated by AXL-induced secretion of lactate through AKT-NF-κB–dependent MCT-1 regulation. Our novel mechanistic findings support future clinical studies to evaluate the therapeutic potential of the AXL inhibitor R428 (BGB324) in highly invasive EAC.

Neoplasia (2018) 20, 1008–1022

Introduction

Esophageal adenocarcinoma (EAC) is a highly aggressive malignancy, and its incidence has increased dramatically in the last few decades in Western countries [1]. Worldwide, an estimated 52,000 individuals are diagnosed with EAC, and 17,460 people will be diagnosed with esophageal cancer in the United States, with EAC comprising the majority of cases [2,3]. EAC is characterized by resistance to chemotherapy and poor prognosis with a 5-year survival rate below 20% [4,5]. Given the dismal clinical outcome of EAC, identification of targetable molecular events that could lead to the development of alternative therapeutic strategies is crucial.

AXL receptor tyrosine kinase (RTK) was originally isolated as a transforming gene from primary human myeloid leukemia cells [6]. Overexpression of AXL has been associated with chemotherapy drug resistance and poor prognosis in EAC [7]. AXL, in the presence of its ligand Gas6, has been shown to drive angiogenesis, proliferation, epithelial-to-mesenchymal transition (EMT), invasiveness, and survival mainly through aberrant activation of downstream phosphoinositide 3-kinase (PI3K)/AKT and mitogen-activated protein kinases (MAPK) pathways [8–11]. Although it is well documented that AXL mediates EMT-induced cell invasion, the precise molecular features underlying this process are not completely characterized.

Cancer-associated lysosomal changes have been implicated in cancer progression and metastatic disease [12,13]. Notably, lysosomal peripheral distribution is emerging as an important feature in cancer cell migration and invasion through enhanced lysosomal exocytosis and extracellular matrix (ECM) degradation [13–16]. Lysosomes are acidic organelles (pH 4.5-5.0) containing over 50 acid hydrolases, among which cathepsins constitute a family of proteases responsible

Address all correspondence to: Abbes Belkhiri, PhD, Vanderbilt University Medical Center, B2211 Medical Center North, 1161 21st Avenue South, Nashville, TN 37232-2730.
E-mail: abbes.belkhiri@vanderbilt.edu

[1] Funding sources: Research reported in this publication was supported by the National Cancer Institute of the National Institutes of Health under Award Number RO1CA193219 and Vanderbilt-Ingram Cancer Center Support Grant (P30CA068485). The content is solely the responsibility of the authors and does not necessarily represent the official views of the National Institutes of Health or Vanderbilt University Medical Center.
Received 25 April 2018; Revised 6 August 2018; Accepted 14 August 2018

1476-5586
https://doi.org/10.1016/j.neo.2018.08.005

for the cleavage of peptide bonds in proteins. Cathepsins are often upregulated in various human cancers and have been implicated in angiogenesis, proliferation, apoptosis, and invasion (reviewed in [17]). The tumor-promoting effects of cathepsins are mainly associated with their secretion and degradation of the ECM. For instance, cathepsin B, which is often localized at the cell surface of cancer cells, enhances cell invasion and metastasis [18,19].

Most cancer cells depend on aerobic glycolysis to generate the energy needed for cellular processes rather than oxidative phosphorylation, a phenomenon termed "the Warburg effect" [20]. This phenomenon is accompanied by increased lactate secretion and metastasis [21,22]. Lactate contributes largely to the acidification of the extracellular pH (pH_e), and it is well known that the pH_e of tumor tissues is often acidic [20]. Acidic pH_e increases not only the activation of some lysosomal proteases with acidic optimal pH but also the expression of some genes facilitating cell invasion. Thus, an acidic microenvironment is strongly associated with tumor metastasis [23] (reviewed in [24]). In addition, it has been proposed that cancer cells adapt to chronic extracellular acidification by upregulating lysosomal proteins expression [25]. Acidification of the tumor microenvironment by lactate secretion is mediated by monocarboxylate transporters (MCTs) that passively transport lactate and protons across the cell membrane [26]. MCT-1, which functions bidirectionally, exports lactic acid from cancer cells [27,28], and increased MCT-1 expression has been associated with higher cancer cell migration, invasion, angiogenesis, and metastasis [22,29–31]. In cancer, MCT-1 expression has been reported to be upregulated by nuclear factor-kappaB (NF-κB) under hypoxia in the absence of functional p53 [32]. Additionally, the NF-κB pathway has been implicated in the activation of *MCT-1* promoter by butyrate in human intestinal epithelial cells [33,34]. Notably, putative NF-κB DNA binding sites were previously reported within the *MCT-1* promoter, and NF-κB has been shown to be regulated by AXL in an AKT-dependent manner [33,34].

Here, we demonstrate that AXL expression in EAC cell lines is implicated in the MCT-1–mediated lactate secretion and extracellular acidification, peripheral distribution of lysosomes, and secretion of cathepsin B, leading to enhanced cell invasiveness. These data establish a novel molecular mechanism by which AXL mediates EAC cell invasion.

Material and Methods

Cell Lines, Antibodies, and Reagents

The human esophageal adenocarcinoma cancer cell lines OE19, OE33, FLO-1, and SK-GT-4 were a kind gift from Dr. David Beer (University of Michigan, Ann Arbor, MI) and were cultured in DMEM (GIBCO) supplemented with 5% fetal bovine serum (FBS; GIBCO) and 1% penicillin/streptomycin (GIBCO), while ESO26 and OAC M5.1 were purchased from Sigma-Aldrich and were cultured in RPMI medium (GIBCO) supplemented with 5% FBS and 1% penicillin/streptomycin. CP-A cells (nondysplastic Barrett's esophagus) were purchased from American Type Culture Collection and cultured in DMEM/F12 medium (GIBCO) supplemented with 140 μg/ml bovine pituitary extract (Sigma), 0.4 μg/ml hydrocortisone (Sigma), 20 ng/ml epidermal growth factor (EGF; Invitrogen), 20 μg/ml adenine (Sigma), 0.1% Insulin-Transferrin-Sodium Selenite supplement (Sigma), and 5% FBS. Antibodies used in this study were as follows: AXL (C44G1), E-cadherin (24E10), Cathepsin B (D1C7Y), AKT (40D4), phospho-(S473)-AKT, NF-κB-p65 (D14E12), phospho-(S536)-NF-κB-p65 (93H1), Tubulin (DM1A) (Cell Signaling Technology); β-actin (AC-74; Sigma-Aldrich); Vimentin (2707-1; Epitomics); LAMP1 (AM8465b-EV; Abgent); phospho-(Y779)-AXL (AF2228; R&D Systems); MCT-1 antibody (AB3538P; Millipore); and ARL8B antibody (GTX44968; GeneTex). The pharmacological inhibitors AXL, R428 (BGB324); NF-κB, BAY 11-7082; and AKT, MK2206 were obtained from Selleckchem. The lysosome anterograde trafficking inhibitor niclosamide was purchased from Selleckchem. The cathepsin B inhibitors, leupeptin and CA-074, were obtained from Sigma-Aldrich and MedChem Express, respectively. MCT-1 inhibitor SR13800 was purchased from Tocris Bioscience.

Lentiviral shRNA-Mediated Silencing

FLO-1 and SK-GT-4 cell lines, both expressing high levels of endogenous AXL, were transduced with a set of five shRNA lentivirus particles (TRCN0000000572, TRCN0000000573, TRCN0000000576, TRCN0000195353, and TRCN0000194971) (Sigma-Aldrich) targeting AXL or a nontarget shRNA in the presence of Polybrene (4 μg/ml; Sigma-Aldrich). Knockdown of CTSB, MCT-1, or ARL8B was performed using the following shRNA lentivirus particles: TRCN0000003658, TRCN0000038340, and TRCN0000296944, respectively (Sigma-Aldrich). Puromycin was added after 48 hours from transduction for 2 weeks to select transductants.

Western Blotting

Cells were washed with ice-cold PBS and harvested using a cell scraper in the presence of RIPA buffer (50 mM Tris-HCl buffer, pH 7.4, 150 mM NaCl, 1% Triton X-100, 1% sodium deoxycholate, and 0.1% SDS) supplemented with 1× proteases inhibitor cocktail and 1× phosphatases inhibitor cocktail (Roche) on ice. Cell lysates were sonicated, clarified by centrifugation at 14,000 rpm for 10 minutes at 4°C, and BCA-assayed for total protein concentration (Pierce, Thermo Scientific). Proteins were resolved on 8%-10% SDS-PAGE and transferred to AmershamTM Protran nitrocellulose membranes (Amersham Biosciences GE Healthcare). Membranes were blocked in Tris-buffered saline Tween 20 (TBST) containing 5% bovine serum albumin (BSA) for 1 hour at room temperature and probed with specific primary antibodies overnight at 4°C. After 4 × 10-minute washes with TBST, membranes were incubated with horseradish peroxidase–conjugated secondary antibodies (Promega) for 1 hour at room temperature and washed 4 × 10 minutes in TBST. Blots were developed using ECL Western blotting detection reagent (Amersham Biosciences GE Healthcare) and signal intensity acquired using ChemiDoc XRS+ (Bio-Rad).

Transwell Invasion Assay

Cells (10^4) were seeded in serum-free medium into the upper chamber of a Corning Matrigel Invasion insert (Fisher Scientific). The insert was then placed in a 24-well plate filled with culture medium containing 5% FBS. After an incubation period of 48 hours, the cells remaining in the upper chamber were scraped using a sterile cotton-tipped applicator, whereas the cells that have invaded through the Matrigel were fixed and stained using the Three-Step Stain Set from Fisher Scientific. The inserts were then imaged using a light microscope and counted using ImageJ software (https://imagej.nih.gov/ij/). For drug treatment experiments, cells were first seeded for 6

hours then treated with R428 (0.2 μM), niclosamide (0.5 μM), leupeptin (20 μM), or CA-074 (10 μM) for 48 hours before being processed for staining and imaging as described above.

Fluorescence Microscopy

Cells were seeded on glass bottom culture dishes (MatTek Corporation) coated with fibronectin and grown to ~80% confluence for 24 hours. For drug treatment experiments, cells were treated with R428 (0.2 μM) or niclosamide (0.5 μM) for 48 hours before being processed for immunofluorescence. Cells were fixed with PBS containing 4% paraformaldehyde for 15 minutes, rinsed in PBS, and permeabilized with 0.1% Triton X-100 in PBS for 5 minutes at room temperature. Fixed cells were blocked with 3% BSA in PBS for 1 hour at room temperature and incubated with a primary antibody (LAMP1, 1:500) diluted in 3% BSA in PBS overnight at 4°C. Dishes were washed 3 × 5 minutes in PBS before being incubated with a species-specific Alexa Fluor 488–conjugated secondary antibody (Thermo Fisher Scientific) (1:500 in 3% BSA in PBS) for 1 hour at room temperature and washed again 3 × 5 minutes in PBS. Nuclei were then stained with DAPI (Cell Biolabs Inc.), and dishes were

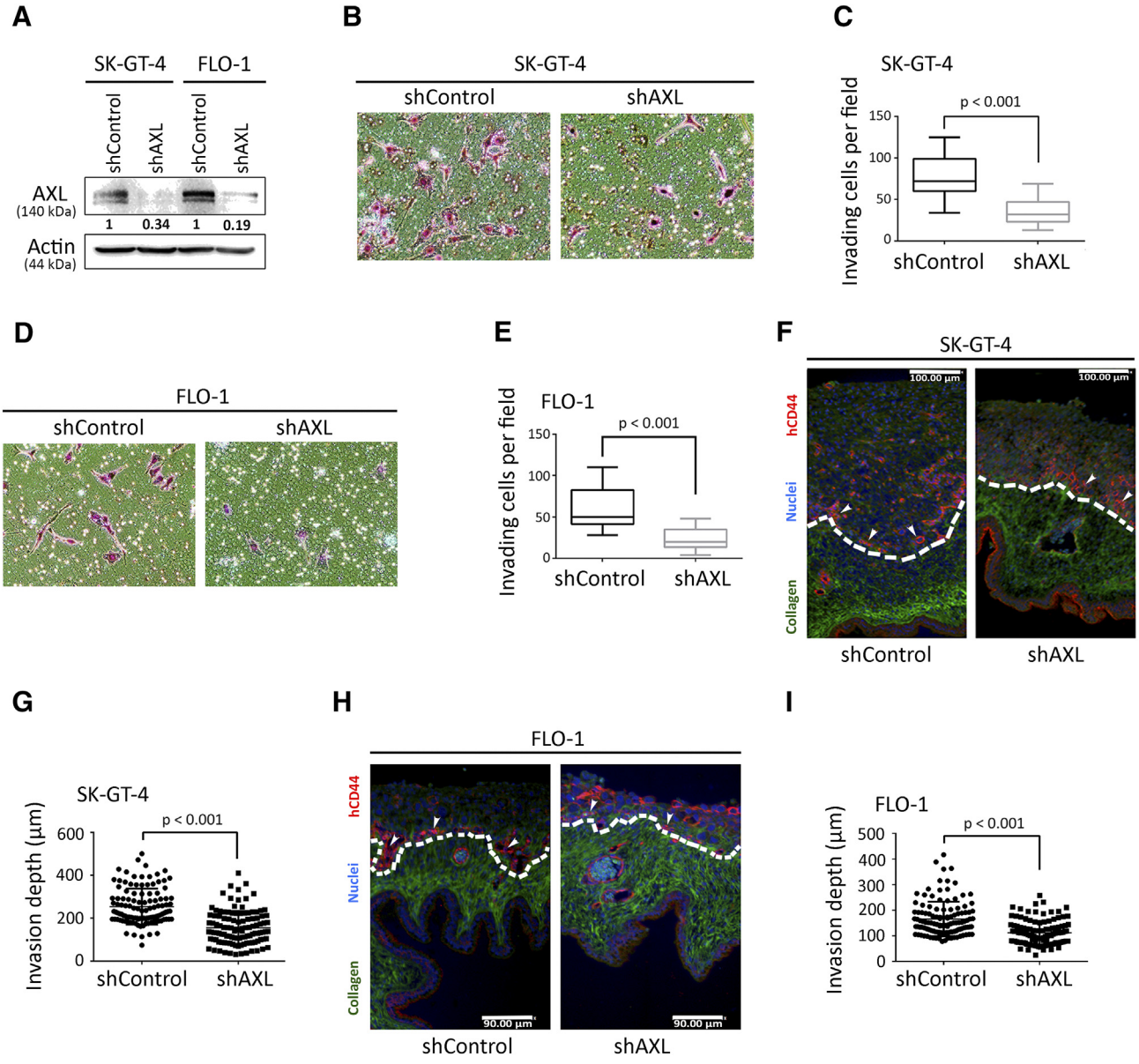

Figure 1. Downregulation of AXL expression in EAC cells impairs invasion *in vitro* and *in vivo*. (A) Western blot analysis of AXL in whole cell lysates from SK-GT-4-shControl, SK-GT-4-shAXL, FLO-1-shControl, or FLO-1-shAXL cells. (B-E) *In vitro* Transwell invasion assay. (B) Transwell invasion assay representative images (20×) of SK-GT-4-shControl versus SK-GT-4-shAXL cells, or (D) FLO-1-shControl versus FLO-1-shAXL cells. (C) Transwell invasion assay quantification as the number of invading SK-GT-4-shControl versus SK-GT-4-shAXL cells, or (E) FLO-1-shControl versus FLO-1-shAXL cells per microscopic field. Data are represented as median ± SD. (F-I) *In vivo* CAM invasion assay. hCD44 in red, collagen in green, and nuclei in blue. The top of the CAM is oriented side up. (F) CAM invasion assay representative images (10×) of SK-GT-4-shControl versus SK-GT-4-shAXL cells, or (H) FLO-1-shControl versus FLO-1-shAXL cells. (G) CAM invasion assay quantification as the invasion depth of SK-GT-4-shControl versus SK-GT-4-shAXL cells, or (I) FLO-1-shControl versus FLO-1-shAXL cells per microscopic field. Data are represented as median ± SD.

mounted with a cover glass using Aqua poly/Mount (Polysciences Inc.). Images were acquired using a laser scanning confocal microscope LSM 880 (Zeiss) with an oil immersion 60× NA 1.49 objective using fluorophore-specific lasers. Lysosomes localization was assessed after a perinuclear region was drawn within one third of the total distance from the nucleus to the plasma membrane. LAMP1-

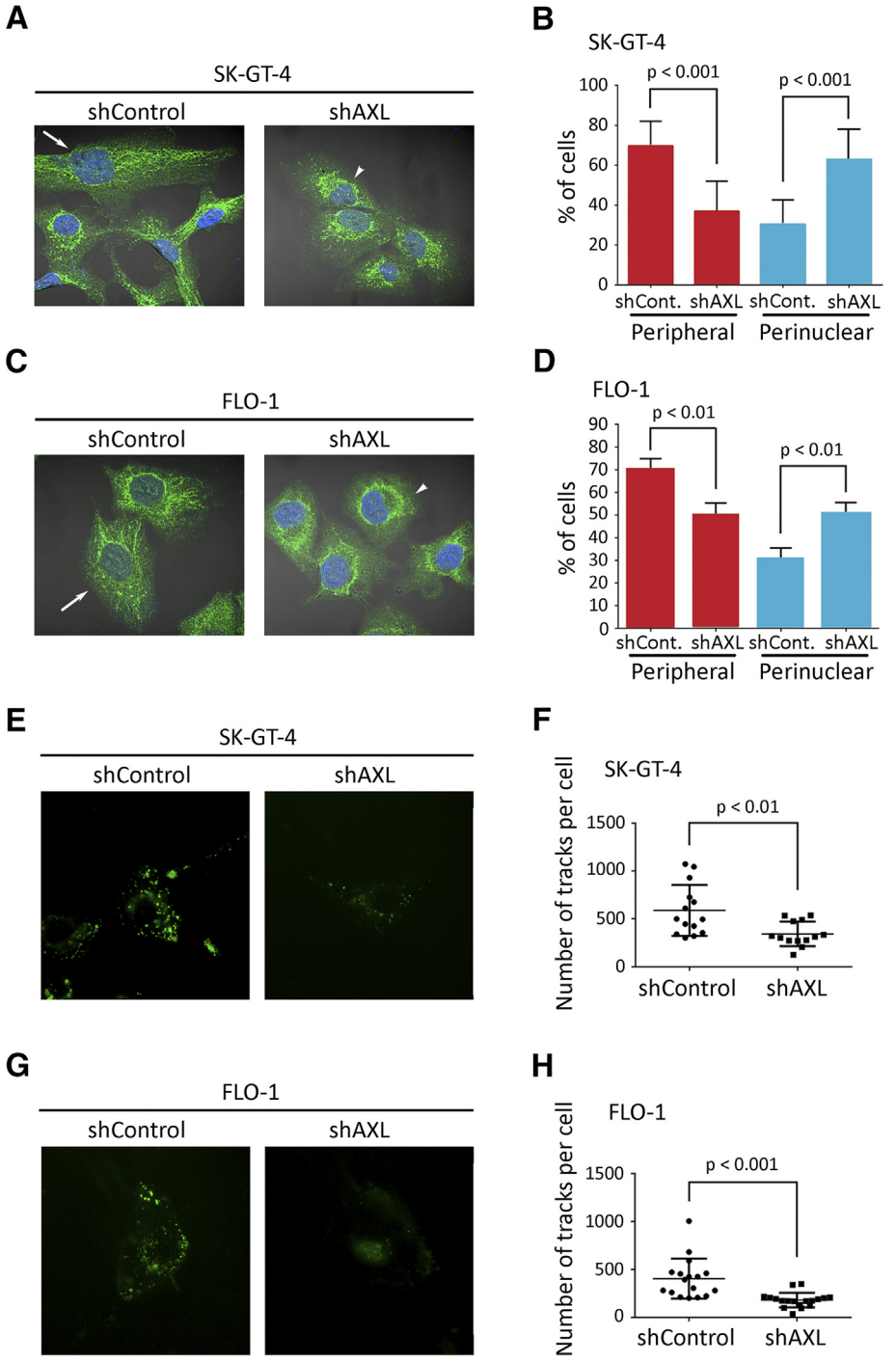

Figure 2. Knockdown of AXL expression decreases peripheral distribution of lysosomes in EAC cells. (A-D) LAMP1 IF analysis. (A) Representative confocal IF images (60×) of LAMP1 (green) in SK-GT-4-shControl versus SK-GT-4-shAXL cells, or (C) FLO-1-shControl versus FLO-1-shAXL cells. Arrows point to cells with peripheral lysosomes, while arrowheads indicate cells with perinuclear lysosomes. (B) Quantification of the percentage of SK-GT-4-shControl versus SK-GT-4-shAXL cells, or (D) FLO-1-shControl versus FLO-1-shAXL cells with either peripheral or perinuclear lysosomes. Data are represented as mean ± SE. (E-H) Live-TIRF microscopy analysis of lysosomes peripheral localization. (E) Representative TIRFM images (60X) of Lysotracker (+) acidic vesicles in SK-GT-4-shControl versus SK-GT-4-shAXL cells, or (G) FLO-1-shControl versus FLO-1-shAXL cells. (F) Quantification of total number of tracks per cell present close to the plasma membrane of SK-GT-4-shControl versus SK-GT-4-shAXL cells, or (H) FLO-1-shControl versus FLO-1-shAXL cells. Data are represented as median ± SD.

positive vesicles that are exclusively located within that region are considered perinuclear, while LAMP1-positive vesicles located beyond that region are considered peripheral.

Total Internal Reflection Fluorescence (TIRF) Microscopy

Cells were seeded on glass-bottom culture dishes (FluoroDish, World Precision Instruments, Inc.) coated with fibronectin and

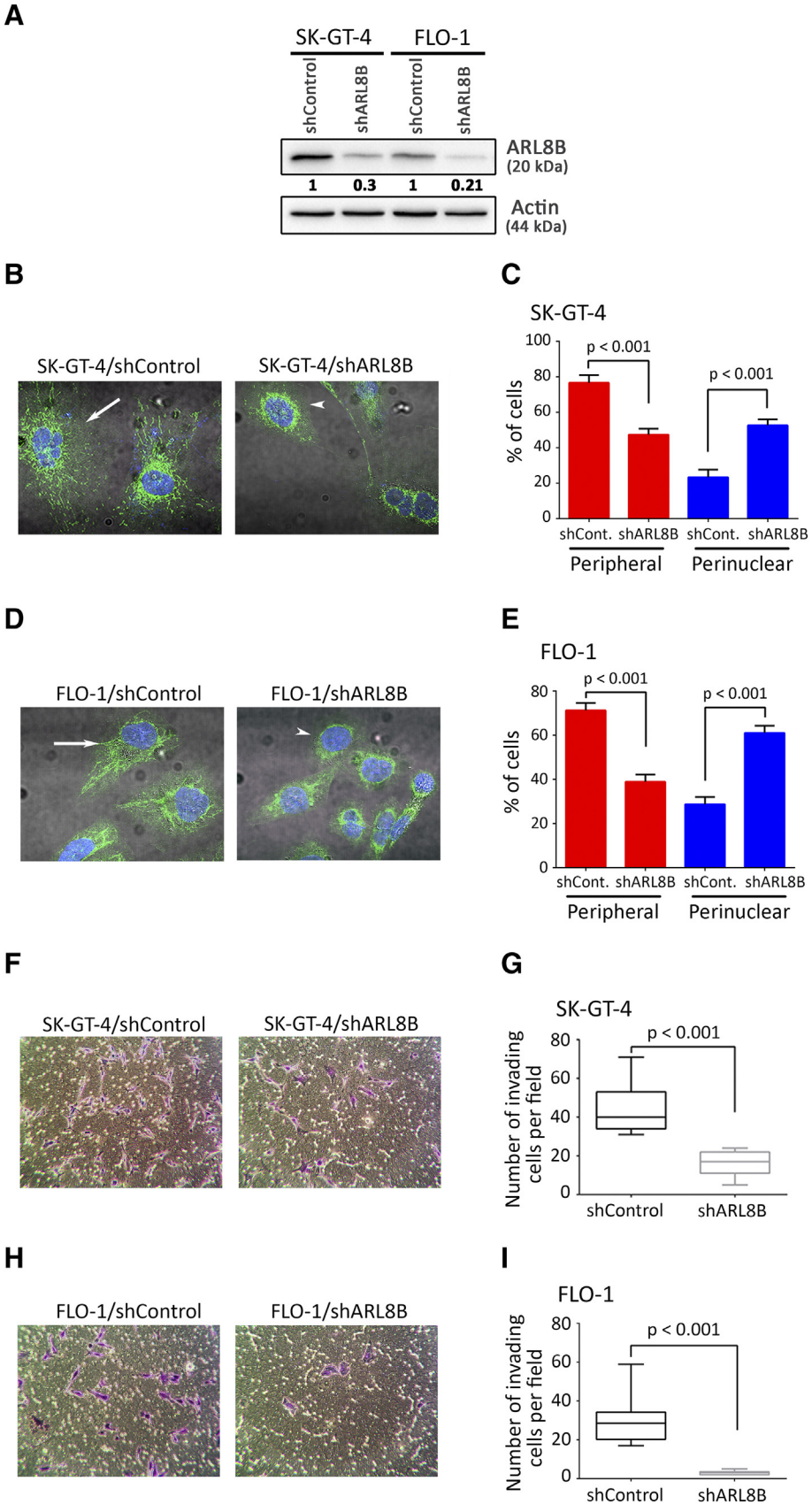

grown to ~80% confluence for 24 hours. Cells were then incubated with Lysotracker Red DND-99 (Invitrogen, Molecular probes) to label acidic organelles according to the manufacturer's instructions. Images were acquired for 30 seconds with no delay using a Ti Eclipse inverted light microscope (Nikon) equipped with a perfect focus, TIRF illuminator (Nikon), a 60× NA 1.49 Apo TIRF objective, and Neo 5.5 cMOS camera (Andro). Automated vesicles tracking analysis was performed using Imaris image processing software (Bitplane).

Chick Chorioallantoic Membrane Assay

Cells (10^6) were grafted on top of "dropped" chorioallantoic membranes (CAM) of 10-day-old chick embryos and allowed to develop for 48 hours at 37°C. CAMs were then harvested and fixed in zinc formalin (Thermo Fisher) for 4 hours before ethanol dehydration and HistoGel embedding (Thermo Scientific). CAM sections (5 μm thick) were prepared from paraffin-embedded samples and processed for immunofluorescence. Antigen retrieval was performed in Modified Dako (Agilent). Aquablock (East Coast Bio) (20%) was used for blocking prior to antibody application for 1 hour at room temperature following manufacturer's instructions. Primary antibody hCD44 (29-7) (1 μg/ml) was obtained as described by Deryugina and Quigley [35] and incubated overnight at 4°C followed by incubation with species-specific Alexa-Fluor secondary antibodies (1:1000, Thermo Fisher) for 2 hours at room temperature. Collagen was stained using CNA-35 Alexa-488 (gift from Erin Rericha, Vanderbilt University) [36,37] for 1 hour at room temperature, and nuclei were stained with Hoechst (2 μg/ml) (Invitrogen) for 15 minutes at room temperature. Slides were then mounted with ProLong Gold Antifade Mountant (Invitrogen). Fluorescent imaging was completed on an Olympus BX61WI upright fluorescent microscope using Volocity Imaging Software. The invasion depth was quantified as a measure of the distance tumor cells traveled into the CAM and was quantified in 4 different fields per image for a total of 30 images.

Cathepsin B Activity Assay

Cells were seeded on fibronectin in a 10-cm culture dish and grown to ~80% confluence for 24 hours, washed two times in PBS and one time in OptiMEM (Life Technologies), and finally incubated with OptiMEM for 48 hours. Conditioned media were collected, and cells were trypsinized, counted, and assessed for cell viability in the presence of trypan blue (Amresco Inc.). Conditioned media were further processed only when cells were >90% viable. Conditioned media were cleared of cells and cell debris by centrifugation at 2000×*g* for 30 minutes at 4°C and then concentrated ~20 times using Amicon Ultra centrifugal filters with a molecular weight cutoff of 3 kDa (Millipore). Cathepsin B activity was then assessed using InnoZymeTM cathepsin B activity assay kit (Millipore) according to the manufacturer's instructions.

TCGA RNA-seq Analysis of Gene Expression in Human EAC Tumors

Publically available RNA-seq data for esophageal cancer from the Cancer Genome Atlas were used to extract gene expression data for 88 esophageal adenocarcinoma primary tumors and 11 esophageal normal tissues. Gene expression was assessed as median absolute RNA counts in EAC tumors or normal tissues.

Extracellular pH Measurement and Lactate Assay

Cells were cultured for up to 72 hours until they reach 100% confluence. Then conditioned media were harvested and pH measured immediately using a benchtop pH meter (accumetTM AE150, Fisher Scientific). The lactate assay was performed according to the manufacturer's instructions (Abcam). Briefly, cells were seeded in triplicate and assayed when confluence reached 70%. Cells were then synchronized by culturing them in serum-free media for 18 hours. Synchronized cells were then starved from glucose for 6 hours and cultured in complete media with glucose in the presence of 2 μM Oligomycin (Sigma Aldrich) for 18 hours. Conditioned media were then harvested, centrifuged for 5 minutes at 14,000 rpm, and subjected to lactate assay. Protein content was determined and used for normalization.

Quantitative Real-Time Reverse Transcriptase Polymerase Chain Reaction (qRT-PCR)

Total RNA was extracted from cells using PureLink RNA Mini Kit (Invitrogen), and cDNA was synthesized using SuperScript cDNA Synthesis Kit (Invitrogen) according to the manufacturer's instructions. Synthesized cDNA was diluted five times, and 2 μl of this dilution was subjected to qRT-PCR. The qRT-PCR was performed with a Bio-Rad CFX Connect Real-time System in a 10-μl reaction volume using iQ SYBR Green Supermix (Bio-Rad) with the following specific primers: *AXL*: forward, 5′-GAAGGTACCATGACAACCCAGGCAAAGTG-3′ and reverse, 5′-GAACTCGAGACGCCATGGGTGCCAAAC-3′; *MCT-1*: forward, 5′-AGGTCCAGTTGGATACACCCC-3′ and reverse, 5′-GCATAAGAGAAGCCGATGGAAAT-3′; *HPRT1*: forward, 5′-ACCCTTTCCAAATCCTCAGC-3′ and reverse, 5′-GTTATGGCGACCCGCAG-3′; *CDH1*: forward, 5′-AGGCCAAGCAGCAGTACATT-3′ and reverse, 5′-ATTCACATCCAGCACATCCA-3′; *CDH2*: forward, 5′-GGTGGAGGAGAAGAAGACCAG-3′ and reverse, 5′-GGCATCAGGCTCCACAGT-3′; *SNAI1*: forward, 5′-CATCCTTCTCACTGCCATG-3′ and reverse, 5′-GTCTTCATCAAAGTCCTGTGG-3′; *SNAI2*: forward, 5′-ATGAGGAATCTGGCTGCTGT-3′ and reverse, 5′-CAGGAGAAAATGCCTTTGGA-3′; *TWIST1*: forward, 5′-TGCATGCATTCTCAAGAGGT-3′ and reverse, 5′-CTATGGTTTTGCAGGCCAGT-3′; *VIM*: forward, 5′-CCTTGAACGCAAAGTGGAATC-3′

Figure 3. Inhibition of lysosomes anterograde trafficking decreases AXL-dependent cell invasion. (A) Western blot analysis of AXL in whole cell lysates from SK-GT-4-shControl, SK-GT-4-shARL8B, FLO-1-shControl, or FLO-1-shARL8B cells. (B-E) LAMP1 IF analysis. (B) Representative confocal IF images (60×) of LAMP1 (Green) in SK-GT-4-shControl versus SK-GT-4-shARL8B cells or (D) FLO-1-shControl versus FLO-1-shARL8B cells. Arrows point to cells with peripheral lysosomes, while arrowheads indicate cells with perinuclear lysosomes. (C) Quantification of the percentage of SK-GT-4-shControl versus SK-GT-4-shARL8B cells or (E) FLO-1-shControl versus FLO-1-shARL8B cells with either peripheral or perinuclear lysosomes. Data are represented as mean ± SE. (F-I) Transwell invasion assay. (F) Transwell invasion assay representative images (20×) of SK-GT-4-shControl versus SK-GT-4-shARL8B cells or (H) FLO-1-shControl versus FLO-1-shARL8B cells. (G) Transwell invasion assay quantification as the number of invading SK-GT-4-shControl versus SK-GT-4-shARL8B cells or (I) FLO-1-shControl versus FLO-1-shARL8B cells per microscopic field. Data are represented as median ± SD.

and reverse, 5′-GACATGCTGTTCCTGAATCTGAG-3′; *CTSB*: forward, 5′-GGCCCCCTGCATCTATCG-3′ and reverse, 5′-AGG TCTCCCGCTGTTCCACTG-3′; *CTSD*: forward, 5′-CCT CCCTGGGTTCAGAAATG-3′ and reverse, 5′-TTCCAATGCAC GAAACAGATCT-3′; *CTSL*: forward, 5′-AGGAGAGCAG TGTGGGAGAA-3′ and reverse, 5′-ATCTGGGGGCCTCA TAAAAC-3′; *CTSK*: forward, 5′-TTCTGCTGC TACCTGTGGTG-3′ and reverse, 5′-GCCTCAAGGTTATG

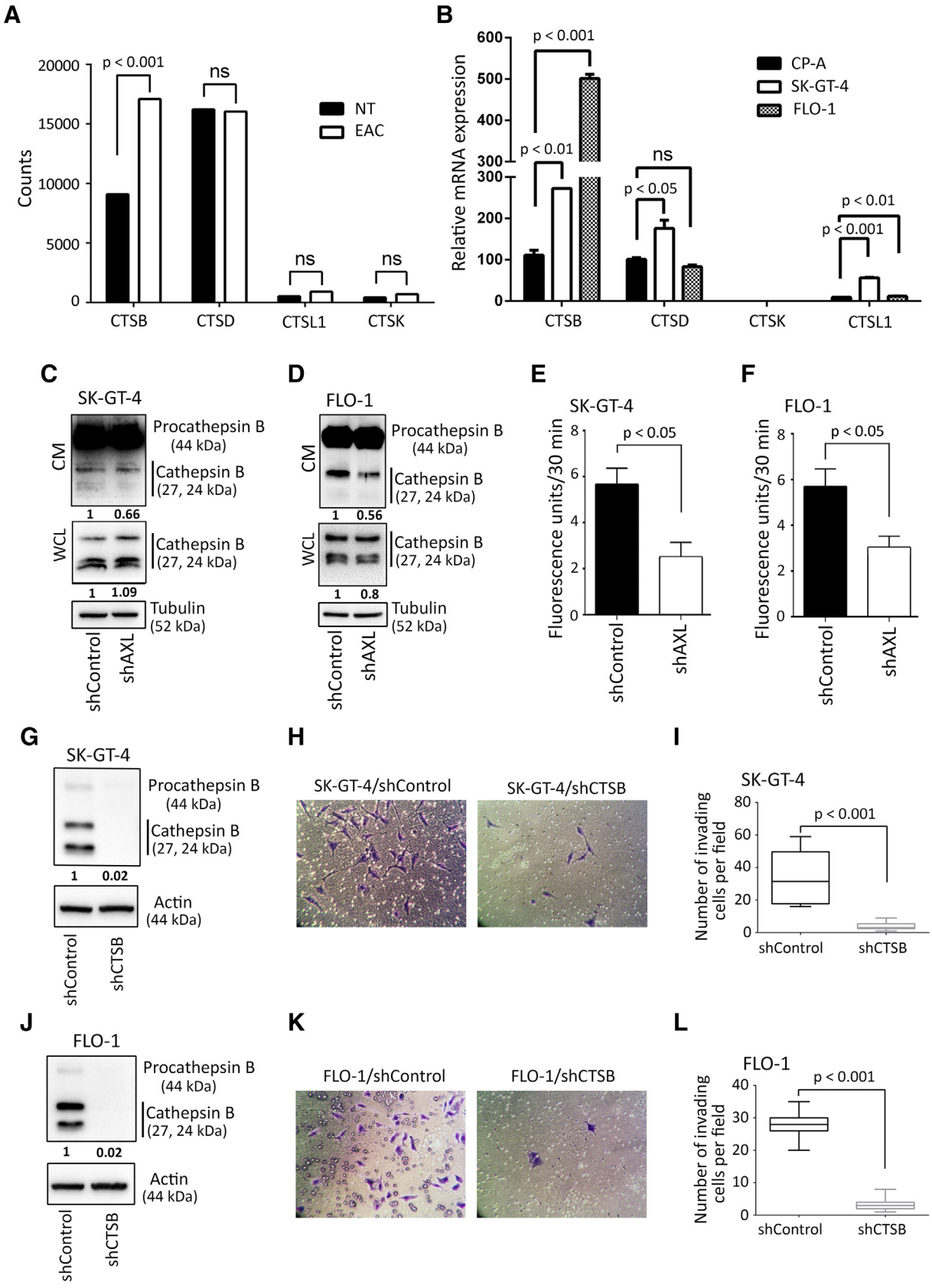

GATGGA-3′; *GAPDH*: forward, 5′-GAAAGCCTGCCGGTGAC TAA-3′ and reverse, 5′-AGGAAAAGCATCACCCGGAG-3′. The threshold cycle number was determined by Bio-Rad CFX manager software version 3.0. Reactions were performed in triplicate, and the threshold cycle numbers were averaged. The data were normalized to the *HPRT1* or *GAPDH* housekeeping genes. The relative mRNA expression levels were calculated according to the formula 2(RT−ET)/ 2(Rn−En), as described previously [38].

Statistical Analysis

Data are expressed as the mean ± SE or ± SD for each condition. Statistical significance was determined using the GraphPad Prism statistical software, and the nonparametric Mann-Whitney test was used for comparisons. Differences with P values ≤ .05 are considered significant.

Results

Association of AXL Expression with EMT and Modulation of EAC Cells Invasion In Vitro and In Vivo

Since EMT is an essential step in invasion and metastasis of cancers [39], we assessed the expression of major EMT-associated genes according to AXL expression in human EAC primary tumors using the publically available TCGA dataset for esophageal cancer. We found a positive association between overexpression of AXL and higher EMT marker genes' expression (Figure S1). In addition, we evaluated the EMT status of a panel of six EAC cell lines by Western blotting of E-cadherin versus vimentin protein expression. Vimentin expression in SK-GT-4, FLO-1, and OAC M5.1 indicated that these cell lines underwent EMT in contrast to OE19, ESO26, and OE33 cell lines that expressed higher levels of E-cadherin. We also found that AXL expression was markedly higher in SK-GT-4 and FLO-1 cells than in the other cell lines (Figure S2*A*). Moreover, this observation was further confirmed by real-time quantitative PCR evaluation of *CDH1* versus *CDH2*, *SNAI1*, *SNAI2*, *TWIST1,* or *VIM* mRNA expression. Overall, consistent higher mesenchymal marker genes' expression was observed in SK-GT-4, FLO-1, and OAC M5.1 (Figure S2, *B-G*). In addition, the *in vitro* Transwell invasion assay data indicated a positive association between AXL expression, EMT, and the invasiveness of EAC cell lines. Indeed, we found that SK-GT-4 and FLO-1 cells were highly invasive ($P < .001$, Figure S2, *H* and *I*).

To ascertain that the SK-GT-4 and FLO-1 cells' invasiveness is dependent on AXL, we knocked down AXL expression in these cells by RNA interference using AXL shRNA or control nontarget shRNA (Figure 1*A*). The Transwell invasion assay data indicated that AXL knockdown significantly impaired the invasiveness of SK-GT-4 cells ($P < .001$, Figure 1, *B* and *C*) or FLO-1 cells ($P < .001$, Figure 1, *D* and *E*) relative to their respective control cells. Moreover, in line with the AXL genetic knockdown data, we found that the pharmacologic inhibition of AXL activity by R428, as indicated by Western blot analysis of p-AXL (Y779) (Figure S3*A*), significantly impaired the invasiveness of SK-GT-4 cells ($P < .05$, Figure S3, *D* and *E*) or FLO-1 cells ($P < .001$, Figure S3, *F* and *G*) in comparison with their respective vehicle-treated cells, without affecting their viability (Figure S3, *B* and *C*).

To corroborate our *in vitro* invasion assay results, we used the CAM *in vivo* assay, as described in Methods. We found that knockdown of AXL expression in SK-GT-4 cells (Figure 1, *F* and *G*) and FLO-1 cells (Figure 1, *H* and *I*) significantly decreased invasion ($P < .001$) into the CAM relative to their respective control cells. Collectively, our results demonstrate that cell invasion *in vitro* and *in vivo* depends on AXL expression.

AXL Expression and Induction of Peripheral Localization of Lysosomes in EAC Cells

Lysosomes localize to the cell periphery in invasive cells, and increased lysosomal exocytosis has been linked to cell invasion [13,14]. To determine whether lysosomes relocate to the cell periphery in the event of AXL expression, we performed IF of the lysosomal marker LAMP-1 and assessed the localization of lysosomes as the percentage of cells with either perinuclear or peripheral lysosomes relative to the total number of examined cells. We found that lysosomes were significantly more peripheral in SK-GT-4-shControl cells than SK-GT-4-shAXL cells ($P < .001$, Figure 2, *A* and *B*) or in FLO-1-shControl cells relative to FLO-1-shAXL cells ($P < .01$, Figure 2, *C* and *D*). Conversely, knockdown of AXL expression significantly increased perinuclear localization of lysosomes in SK-GT-4 cells ($P < .001$, Figure 2, *A* and *B*) and FLO-1 cells ($P < .01$, Figure 2, *C* and *D*) relative to their respective control cells. In agreement with these data, the pharmacologic inhibition of AXL by R428 (0.2 μM) significantly decreased peripheral and increased perinuclear localization of lysosomes in SK-GT-4 cells ($P < .001$, Figure S3, *H* and *I*) and FLO-1 cells ($P < .01$, Figure S3, *J* and *K*) relative to their respective vehicle-treated control cells. The inhibition of AXL by R428 in both cell lines was confirmed by Western blot analysis of p-AXL (Y779) (Figure S3*A*). To further confirm that lysosomes are more peripheral in cells expressing high levels of AXL, lysosomes were labeled with LysoTracker and live-imaged using total internal reflection fluorescence (TIRF) microscopy, which allows the visualization of lysosomes that are present at the cell periphery [40]. We found a significantly higher number of peripheral lysosomes in SK-GT-4-shControl cells relative to SK-GT-4-shAXL cells ($P < .01$, Figure 2, *E* and *F*, Video S1) or in FLO-1-shControl cells in comparison with FLO-1-shAXL cells ($P < .001$, Figure 2, *G* and *H*, Video S2), as indicated by automated tracking of the number of lysosome tracks per cell. Taken together, these data strongly suggest that AXL expression promotes peripheral localization of lysosomes in these EAC cell lines.

Figure 4. Downregulation of AXL expression impairs cathepsin B secretion and cell invasion in EAC cells. (A) Cathepsins' median expression in a panel of 88 EAC primary tumors versus 11 esophageal normal tissues (NT) from the TCGA RNA-Seq data. (B) Cathepsins' relative mRNA expression in premalignant nondysplastic Barrett's CP-A cell line versus SK-GT-4 and FLO-1 EAC cell lines. (C) Western blot analysis of cathepsin B in conditioned media (CM) or whole cell lysates (WCL) from SK-GT-4-shControl versus SK-GT-4-shAXL cells, or (D) FLO-1-shControl versus FLO-1-shAXL cells. (E-F) Cathepsin B activity assay in CM. (E) Cathepsin B activity in CM from SK-GT-4-shControl versus SK-GT-4-shAXL cells, or (F) FLO-1-shControl versus FLO-1-shAXL cells. (G) Western blot analysis of cathepsin B in WCL from SK-GT-4-shControl versus SK-GT-4-shCTSB, or (J) FLO-1-shControl versus or FLO-1-shCTSB cells. (H-I; K-L) Transwell invasion assay. (H) Transwell invasion assay representative images (20×) of SK-GT-4-shControl versus SK-GT-4-shCTSB cells or (K) FLO-1-shControl versus FLO-1-shCTSB cells. (I) Transwell invasion assay quantification as the number of invading SK-GT-4-shControl versus SK-GT-4-shCTSB cells or (L) FLO-1-shControl versus FLO-1-shCTSB cells per microscopic field. Data are represented as mean ± SE or median ± SD.

Inhibition of Lysosomes Anterograde Trafficking and Impairment of AXL-Dependent Cell Invasion in EAC Cells

Peripheral localization of lysosomes upon oncogene transformation is likely to promote lysosomal exocytosis and consequently cell invasion through ECM degradation [13–15]. To investigate whether peripheral localization of lysosomes is required for AXL-dependent cell invasion, anterograde trafficking of lysosomes was inhibited by knocking down of ARL8B expression using RNA interference [41–43]. Knockdown of ARL8B in SK-GT-4 and FLO-1 cells was confirmed by Western blot analysis (Figure 3*A*). Indeed, assessment of LAMP-1–positive lysosomes

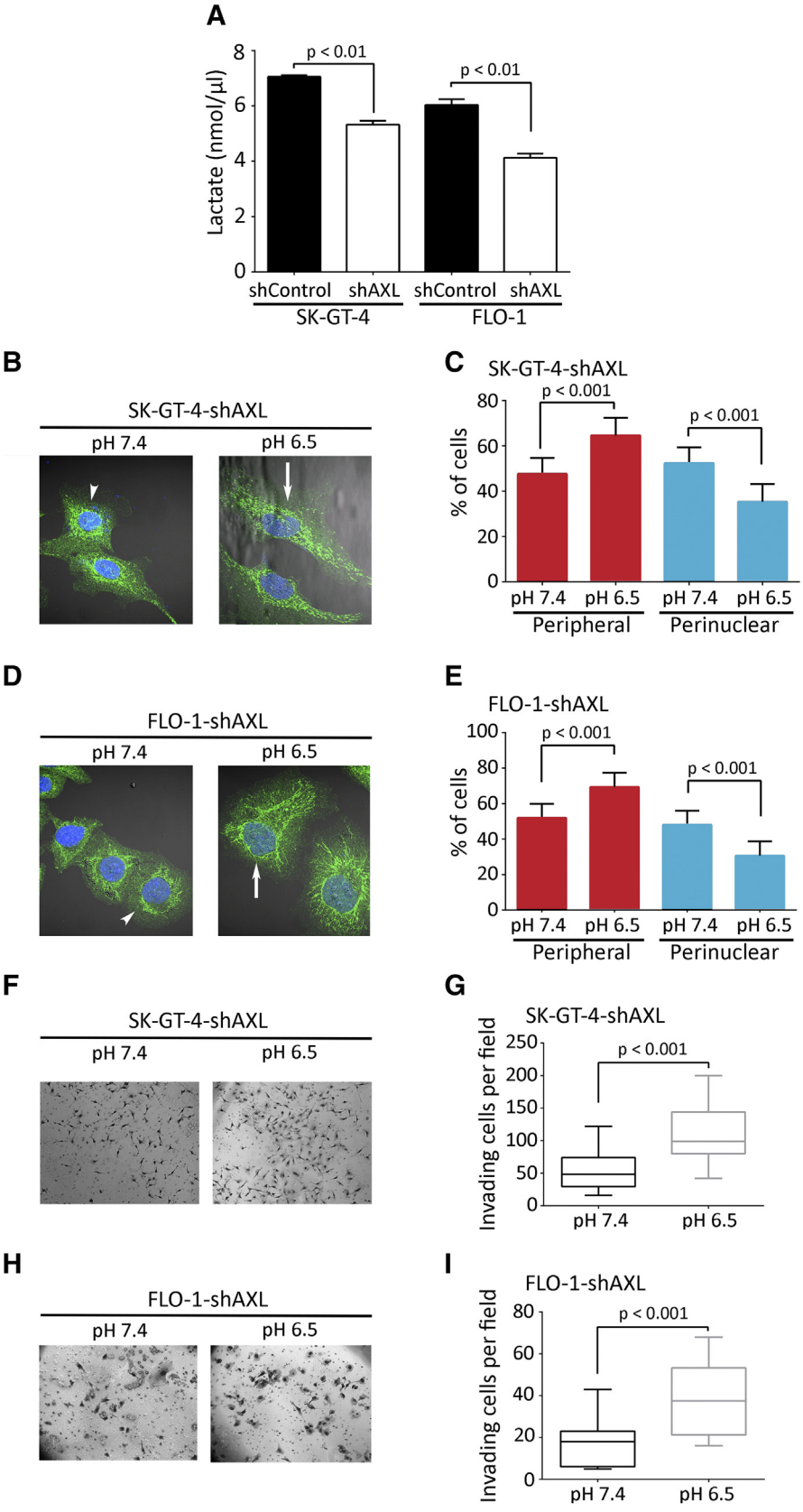

localization revealed that knockdown of ARL8B expression significantly increased the percentage of cells with perinuclear lysosomes and decreased the fraction of those with peripheral lysosomes in SK-GT-4 cells ($P < .001$, Figure 3, *B* and *C*) and FLO-1 cells ($P < .001$, Figure 3, *D* and *E*) compared to their respective control cells. Interestingly, downregulation of ARL8B expression also significantly reduced the invasion of SK-GT-4 cells by ~2-folds ($P < .001$, Figure 3, *F* and *G*) and FLO-1 cells by ~5-folds ($P < .001$, Figure 3, *H* and *I*) compared to their respective control cells, as assessed by *in vitro* Transwell invasion assay. To further support these data, anterograde trafficking of lysosomes was blocked using niclosamide [44]. Treatment of SK-GT-4 ($P < .001$, Figure S4, *A* and *B*) or FLO-1 ($P < .001$, Figure S4, *C* and *D*) parental cells with niclosamide (0.5 μM) significantly decreased the fraction of peripheral lysosomes relative to their respective vehicle-treated control cells as assessed by IF of LAMP1. Conversely, niclosamide significantly increased the perinuclear fraction of lysosomes in SK-GT-4 cells ($P < .001$, Figure S4, *A* and *B*) and in FLO-1 cells ($P < .001$, Figure S4, *C* and *D*) compared to their respective vehicle-treated cells. Additionally, analysis of cell invasion *in vitro* through Matrigel revealed that inhibition of anterograde trafficking of lysosomes using niclosamide significantly decreased the invasiveness of SK-GT-4 cells ($P < .01$, Figure S4, *E* and *F*) and FLO-1 cells ($P < .001$, Figure S4, *H* and *I*) in comparison with their respective vehicle-treated cells. The cell viability was not affected by niclosamide after treatment of either SK-GT-4 cells (Figure S4*G*) or FLO-1 cells (Figure S4*J*). Taken together, these results strongly suggest that the peripheral lysosomal localization is required for AXL-dependent cell invasion.

Cell Invasion Mediation by AXL through Regulation of Cathepsin B Secretion in EAC Cells

Lysosomal exocytosis of hydrolases is likely to facilitate ECM degradation, invasion, and cancer progression [13–15]. To identify lysosomal exocytosis of candidate cathepsins in EAC cells, we mined publicly available RNA-seq data for EAC from the Cancer Genome Atlas (TCGA) and extracted the expression levels of key cathepsins involved in cancer progression. Our analysis identified cathepsin B to be highly expressed in EAC primary tumors and differentially overexpressed relative to normal esophageal tissues ($P < .001$, Figure 4*A*). Expression levels of these cathepsins were further examined in our EAC cell lines by real-time quantitative PCR and contrasted to their expression in a premalignant nondysplastic Barrett's esophagus cell line CP-A. Consistent with the TCGA data, we found that cathepsin B was highly expressed compared to the other cathepsins in SK-GT-4 and FLO-1 cells relative to CP-A cells (Figure 4*B*). To investigate whether cathepsin B secretion is regulated by AXL, serum-free conditioned media (CM) from SK-GT-4-shAXL cells, FLO-1-shAXL cells, or their respective shControl cells were concentrated and normalized for equal cell number then analyzed by Western blot to evaluate levels of secreted cathepsin B proteins. We found that cathepsin B was mostly secreted as a proform (procathepsin B) and to a lesser extent as active cathepsin B. Moreover, the data revealed that knockdown of AXL expression reduced active cathepsin B secretion by approximately 50% in SK-GT-4 cells (Figure 4*C*) as well as FLO-1 cells (Figure 4*D*) in comparison with their respective control cells. To corroborate these data, the same serum-free conditioned media were used to assess the enzymatic activity of secreted cathepsin B. As expected, knockdown of AXL expression significantly decreased cathepsin B activity by 50% in SK-GT-4 cells ($P < .05$, Figure 4*E*) and by 30% in FLO-1 cells ($P < .05$, Figure 4*F*) relative to their respective control cells. Notably, our Western blot data showed that knockdown of AXL expression in SK-GT-4 and FLO-1 cells had no significant effect on the expression levels of intracellular cathepsin B proteins (Figure 4, *C* and *D*).

Secretion of cathepsin B has been reported to promote cell invasion [18,45,46]. Therefore, we tested whether cathepsin B is required for AXL-dependent cell invasion by knocking down cathepsin B expression using RNA interference. Effective downregulation of cathepsin B expression in SK-GT-4 (Figure 4*G*) and FLO-1 cells (Figure 4*J*) was confirmed by Western blot analysis. The Transwell invasion assay data revealed that knockdown of cathepsin B expression significantly impaired AXL-dependent invasion in SK-GT-4 cells ($P < .001$, Figure 4, *H* and *I*) or FLO-1 cells ($P < .001$, Figure 4, *K* and *L*) relative to their respective control cells. Additionally, cell invasion was assessed in the context of cathepsin B activity inhibition using either leupeptin (20 μM) or CA-074 (10 μM) [47]. We found that inhibition of cathepsin B activity significantly impaired AXL-dependent invasion in SK-GT-4 cells ($P < .001$, Figure S5, *A*, *B*, *G* and *H*) or FLO-1 cells ($P < .001$, Figure S5, *D*, *E*, *J* and *K*) relative to their respective vehicle-treated cells. The cell viability assay results showed that leupeptin- or CA-074–induced suppression of cell invasion was not due to cytotoxicity effects in both SK-GT-4 cells (Figure S5, *C* and *F*) or FLO-1 cells (Figure S5, *I* and *L*). Our data strongly suggest that active cathepsin B secretion is required for AXL-dependent cell invasion.

Peripheral Localization of Lysosomes and Cell Invasion Mediation by AXL through Regulation of Extracellular Acidification

Acidic extracellular pH (pH_e) induces a peripheral distribution of lysosomes in cancer cells [48,49]. We investigated whether AXL-dependent lysosomes peripheral distribution is dependent on extracellular acidification. We found that pH values of the CM from SK-GT-4-shAXL (pH 6.9) or FLO-1-shAXL (pH 6.8) cells were slightly less acidic than those from SK-GT-4-shControl (pH 6.6) or FLO-1-shControl (pH 6.6) cells (Figure S6). Since lactate secretion is the major contributor to the acidification of the extracellular microenvironment,

Figure 5. AXL expression mediates lysosomes peripheral distribution and cell invasion through lactate secretion and extracellular acidification. (A) Lactate assay measuring lactate secretion in the CM of SK-GT-4-shControl versus SK-GT-4-shAXL cells or FLO-1-shControl versus FLO-1-shAXL cells. (B-E) LAMP1 IF analysis. (B) Representative confocal IF images (60×) of LAMP1 (green) in SK-GT-4-shAXL cells, or (D) FLO-1-shAXL cells cultured in either pH 7.4 or pH 6.5. Arrows point to cells with peripheral lysosomes, while arrowheads indicate cells with perinuclear lysosomes. (C) Quantification of the percentage of SK-GT-4-shAXL or (E) FLO-1-shAXL cells with either peripheral or perinuclear lysosomes relative to their respective total cell number after culturing in pH 7.4 or pH 6.5. Data are represented as mean ± SE. (F-I) Transwell invasion assay. (F) Transwell invasion assay representative images (20×) of SK-GT-4-shAXL cells or (H) FLO-1-shAXL cells cultured in pH 7.4 or pH 6.5. (G) Transwell invasion assay quantification as the number of invading SK-GT-4-shAXL cells or (I) FLO-1-shAXL cells per microscopic field after culturing in pH 7.4 or pH 6.5. Data are represented as median ± SD.

we assessed the amount of lactate in the CM of these cells. Consistent with the pH_e measurement data (Figure S6), lactate secretion was 25% higher in SK-GT-4-shControl cells (7.06 nmol/μl) relative to SK-GT-4-shAXL cells (5.32 nmol/μl, $P < .01$, Figure 5*A*) and 30% higher in FLO-1-shControl cells (6.04 nmol/μl) in comparison with FLO-1-shAXL cells (4.12 nmol/μl, $P < .01$, Figure 5*A*).

To ascertain that AXL-induced acidification of the CM is responsible for the peripheral distribution of lysosomes and the consequent increase in cell invasion, SK-GT-4-shAXL or FLO-1-shAXL cells that displayed less acidic pH_e were cultured in physiological (pH 7.4) or acidic pH (pH 6.5) and assessed for lysosomes distribution by IF of LAMP1 and cell invasion *in vitro*. We found that culturing the cells in acidic pH significantly increased the proportion of cells with peripheral lysosomes and decreased the percentage of cells with perinuclear lysosomes relative to SK-GT-4-shAXL ($P < .001$, Figure 5, *B* and *C*) and FLO-1-shAXL ($P < .001$, Figure 5, *D* and *E*) cultured at pH 7.4. Additionally, culturing SK-GT-4-shAXL or FLO-1-shAXL cells in acidic pH significantly increased their invasiveness *in vitro* by ~2-folds compared to the cells cultured in physiological pH ($P < .001$, Figure 5, *F* and *G*, and *H* and *I*, respectively). Collectively, these results suggest that AXL mediates peripheral distribution of lysosomes and cell invasion through regulation of extracellular acidification.

Promotion of Lactate Secretion and Cell Invasion by AXL through Regulation of MCT-1 Expression

Acidification of the tumor microenvironment by lactate secretion is controlled by monocarboxylate transporters, and it has been reported that MCT-1 can transport lactate into and out of tumor cells [27,28]. To determine whether AXL-induced lactate secretion is dependent on MCT-1, we downregulated MCT-1 expression using RNA interference (Figure 6*A*). We found that downregulation of MCT-1 expression decreased the amount of lactate secreted in the CM of SK-GT-4 cells or FLO-1 cells by ~30% relative to their respective control cells (Figure 6*B*). Additionally, assessment of cell invasion *in vitro* revealed that MCT-1 knockdown significantly impaired the invasiveness of SK-GT-4 cells ($P < .001$, Figure 6, *C* and *D*) or FLO-1cells ($P < .001$, Figure 6, *E* and *F*) compared to their respective control cells. Moreover, we inhibited the activity of MCT-1 using SR13800 (1 μM) and assessed the amount of lactate in the CM of our EAC cell models. We found that MCT-1 inhibition significantly decreased lactate secretion by 30% in SK-GT-4 cells (4.96 nmol/μl) relative to control cells (7.16 nmol/μl) ($P < .01$, Figure S7*A*) and by 50% in FLO-1 cells (3.21 nmol/μl) in comparison with control cells (6.58 nmol/μl) ($P < .01$, Figure S7*A*). Furthermore, we found that inhibition of MCT-1 activity significantly impaired the invasiveness of SK-GT-4 cells ($P < .001$, Figure S7, *B* and *C*) as well as FLO-1 cells ($P < .001$, Figure S7, *D* and *E*) compared to their respective control cells without affecting their viability (Figure S7*F*). We next investigated whether AXL regulates MCT-1 expression using real-time RT-PCR and Western blotting. We found that the mRNA levels of *MCT-1* were significantly lower in SK-GT-4-shAXL ($P < .05$, Figure 6, *G* and *H*) or FLO-1-shAXL ($P < .05$, Figure 6, *I* and *J*) compared to their respective control cells. Moreover, MCT-1 protein expression was also decreased in SK-GT-4-shAXL (Figure 6*K*) or FLO-1-shAXL (Figure 6*L*) relative to their respective control cells. Collectively, these data suggest that AXL induced-lactate secretion may involve regulation of mRNA and protein expression of MCT-1.

Up-regulation of MCT-1 Expression by AXL through Regulation of the AKT-NF-κB Signaling Pathway

Based on the published reports indicating that MCT-1 expression is upregulated by NF-κB [32,50] and that AXL activates NF-κB pathway through AKT [34], we hypothesized that AXL could upregulate MCT-1 expression through regulation of AKT-NF-κB signaling axis. In fact, we found that both AKT and NF-κB pathways are downregulated in SK-GT-4-shAXL (Figure 7*A*) and FLO-1-shAXL (Figure 7*B*) compared to their respective control cells as assessed by Western blotting of p-AKT (S473) and p-NF-κB-p65 (S536). We next investigated whether pharmacological inhibition of NF-κB or AKT pathways could decrease MCT-1 protein expression. Indeed, inhibition of either NF-κB using BAY 11-7082 (5 μM) or AKT using MK2206 (20 μM) markedly downregulated MCT-1 protein expression in SK-GT-4 cells (Figure 7*C*) or FLO-1 cells (Figure 7*D*) relative to their respective control cells. Notably, inhibition of NF-κB using BAY (5 μM) downregulated *MCT-1* mRNA expression in both SK-GT-4 cells (Figure 7*E*) and FLO-1 cells (Figure 7*F*) compared to their respective control cells. Our findings indicate that AXL upregulates MCT-1 expression through regulation of the AKT-NF-κB signaling pathway in EAC cells.

Discussion

Although the role of AXL in cancer cell invasion has been established, the underlying mechanism remains unclear. Our results show that AXL overexpression is related to an EMT phenotype, an aggressive feature of invasion and metastasis in EAC. We found that AXL overexpression is associated with higher expression of major EMT marker genes in human EAC primary tumors and cell lines. In fact, AXL was shown to be a downstream effector of EMT that is required for breast cancer metastasis [9]. In addition, AXL functions as an effector of vimentin-dependent breast cancer cell migration during EMT [51].

We found that AXL expression is concomitant with a peripheral distribution of lysosomes and knockdown of AXL expression redistributes lysosomes to a more perinuclear location. Our findings are consistent with other studies showing that transformation and cancer progression induce a series of changes in lysosomes function and an increase in the peripheral distribution of lysosomes [12]. Lysosomes travel along the two-way microtubule tracks and reach the cell periphery through the microtubule anterograde trafficking, which is regulated by the PI3K pathway and the GTPase RhoA [49]. Our data involve AXL expression in the regulation of peripheral localization of lysosomes and cell invasion, suggesting that the two events have a causal relationship. Indeed, cancer-associated peripheral distribution of lysosomes is emerging as important for cell migration and invasion [15]. Consistent with Dykes and colleagues, we found that mesenchymal EAC cell lines expressing high levels of AXL display enhanced anterograde lysosome trafficking and that inhibition of lysosome trafficking by knocking down AXL does not seem to reverse EMT (data not shown) but does inhibit EMT-mediated cell invasion [52]. Moreover, we showed that inhibition of AXL-dependent peripheral distribution of lysosomes by knocking down of ARL8B expression or using niclosamide strongly impairs cell invasion, demonstrating that AXL-mediated cell invasion requires an effective trafficking of lysosomes to the cell periphery. We postulated that peripheral distribution of lysosomes may be accompanied by enhanced lysosomal exocytosis. Indeed, we observed that AXL expression increases secretion of the active form of cathepsin B in the

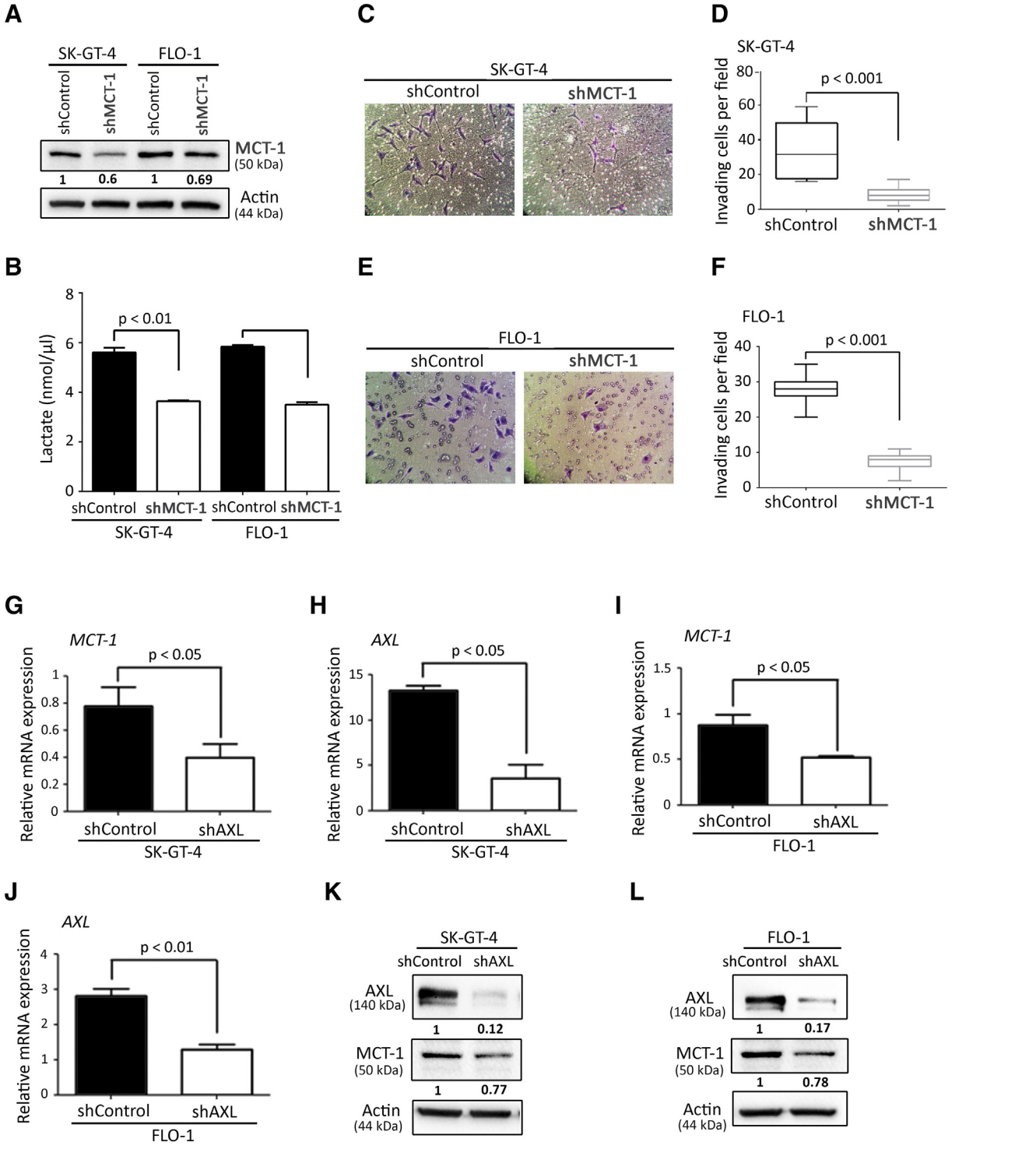

Figure 6. AXL-induced lactate secretion and cell invasion depends on MCT-1 activity. (A) Western blot analysis of MCT-1 in whole cell lysates from SK-GT-4-shControl, SK-GT-4-shMCT-1, FLO-1-shControl, and FLO-1-shMCT-1 cells. (B) Lactate assay measuring lactate secretion in the CM of SK-GT-4-shControl versus SK-GT-4-shMCT-1 cells or FLO-1-shControl versus FLO-1-shMCT-1 cells. (C-F) Transwell invasion assay. (C) Transwell invasion assay representative images (20×) of SK-GT-4-shControl versus SK-GT-4-shMCT-1 cells or (E) FLO1-shControl versus FLO-1-shMCT-1 cells. (D) Transwell invasion assay quantification as the number of invading SK-GT-4-shControl versus SK-GT-4-shMCT-1 cells or (F) FLO-1-shControl versus FLO-1-shMCT-1 cells. Data are represented as median ± SD. (G-J) Real-time quantitative PCR analysis of *MCT-1* and *AXL* mRNA expression in SK-GT-4-shControl versus SK-GT-4-shAXL (G and H), and in FLO-1-shControl versus FLO-1-shAXL (I and J). Data are represented as mean ± SD. (K-L) Western blot analysis of MCT-1 and AXL protein expression in SK-GT-4-shControl versus SK-GT-4-shAXL (K), and in FLO-1-shControl versus FLO-1-shAXL (L).

conditioned media of EAC cells. Notably, the secretion of the proform of cathepsin B remained high and unaffected by downregulation of AXL expression in these cells. In fact, tumor cells secrete both procathepsin B and active cathepsin B, and the secretion of procathepsin B occurs principally as a result of increased expression in cancer cells [53]. Our data suggest that AXL regulates

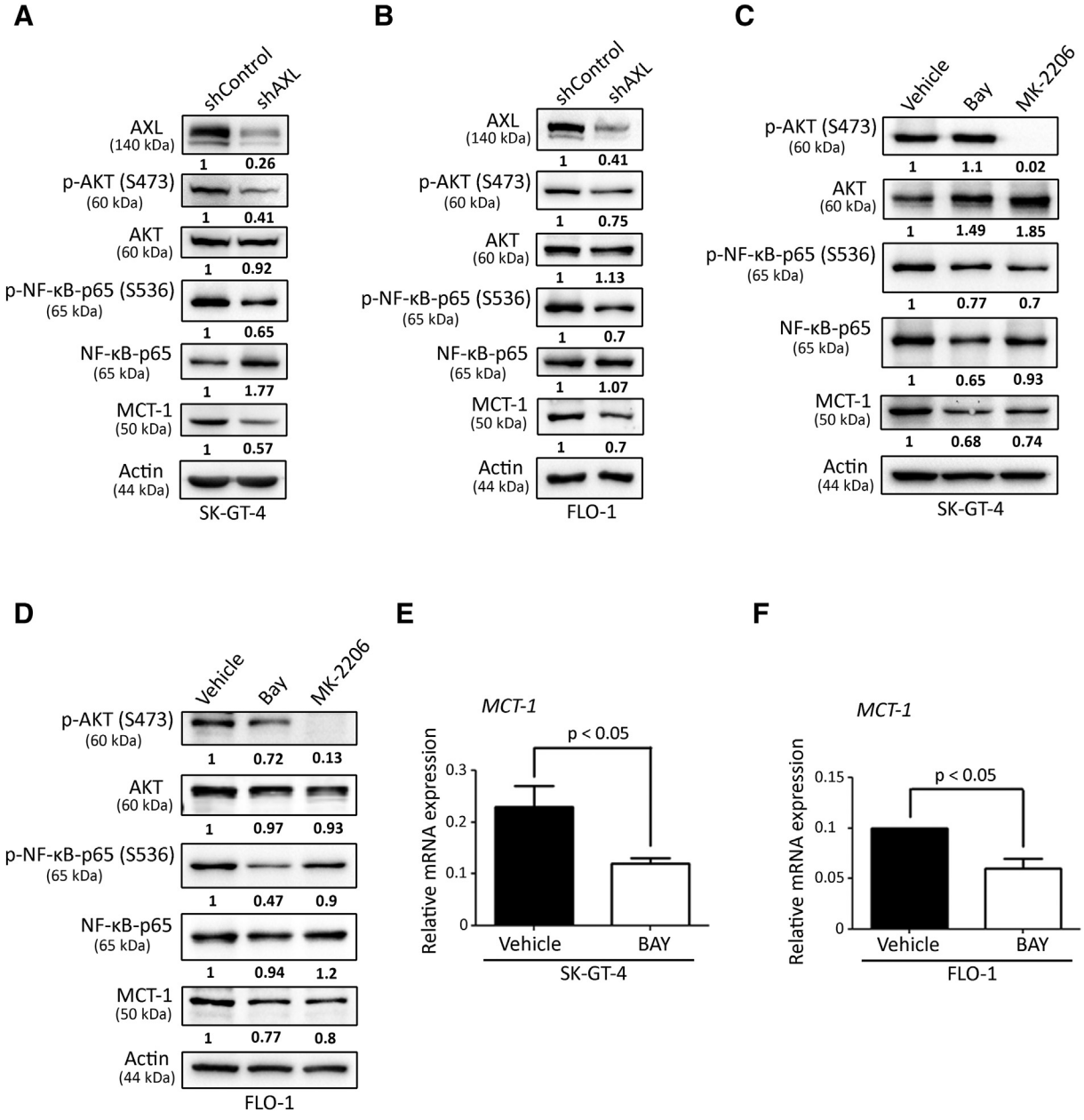

Figure 7. AXL-dependent activation of the AKT-NF-κB pathway is required for upregulation of MCT-1 expression. (A-B) Western blot analysis of AXL, p-AKT (S473), total AKT, p-NF-κB-p65(S536), total NF-κB-p65, and MCT-1 in SK-GT-4-shControl cells (A) or FLO-1-shControl cells (B) versus their respective shAXL cells. (C-D) Western blot analysis of p-AKT (S473), total AKT, p-NF-κB-p65(S536), total NF-κB-p65, and MCT-1 in SK-GT-4 control cells (C) or FLO-1 control cells (D) versus their respective BAY- or MK2206-treated cells. (E-F) Real-time quantitative PCR analysis of *MCT-1* mRNA expression in SK-GT-4 control cells (E) or FLO-1 control cells (F) versus their respective BAY-treated cells. Data are represented as mean ± SD.

active cathepsin B secretion but not its expression. It is well established that cathepsins trafficked to the cell periphery or secreted via exocytosis of peripheral lysosomes augment cell invasion through ECM remodeling [54–56]. Consistent with other studies, we found that inhibition of cathepsin B expression and activity strongly impairs AXL-dependent cell invasion, further demonstrating the need for active cathepsin B to maintain cell invasion [18].

Several studies indicate that extracellular acidification induces lysosomes redistribution to the cell periphery [48,49]. Extracellular acidification is often observed in the tumor microenvironment, and lactate secretion is the major contributor to this effect [57]. In line with these studies, our data show that AXL expression and dependent cell invasion are associated with increased extracellular acidity as well as lactate secretion in EAC cells. It is well established that acidification of the tumor microenvironment by lactate secretion is mediated by MCTs that passively transport lactate and protons across the cell membrane [26]. Increased expression of MCT-1, which exports lactate from cancer cells, has been involved in cancer cell migration, invasion, angiogenesis, and metastasis [22,27–31]. In fact, our data indicate that MCT-1 is required for the secretion of lactate and cell invasion in AXL-expressing EAC cells, as knockdown or pharmacological inhibition of MCT-1 impairs these effects. Mechanistic investigations showed that MCT-1 expression is upregulated by AXL through activation of the AKT-NF-κB signaling pathway in EAC

cells. Pharmacological inhibition of NF-κB reduced MCT-1 protein and mRNA expression, suggesting transcriptional regulation of *MCT-1* by NF-κB. In support of this finding, Cuff and Beechey have previously identified NF-κB putative binding sites in the *MCT-1* promoter region [33]. Further studies will be required to validate these transcription binding sites. Collectively, our findings suggest that AXL-dependent lactate secretion could be the result of increased MCT-1 expression. However, we cannot exclude that the increase in lactate secretion could be due to enhanced aerobic glycolysis activity in AXL-expressing EAC cells, a common feature of glycolytic cancer cells known as the "Warburg Effect" [20].

AXL-dependent extracellular acidity could play a key role in the activation of secreted cathepsin B leading to cell invasion. It is proposed that an acidic pHe increases the activation of some lysosomal proteases with acidic optimal pH, thereby promoting the degradation of the ECM, cell migration, and invasion (reviewed in [24]). We and others have observed that acidic pH_e appears to transduce an intracellular signaling that activates the anterograde trafficking machinery, thereby enhancing lysosome peripheral distribution and exocytosis [48,49]. However, the underlying molecular mechanisms remain unknown.

RTKs have been shown to stimulate lysosomes trafficking, protease secretion, and cell invasion by distinct molecular mechanisms. Indeed, HGF and its receptor MET have been reported to induce anterograde trafficking of lysosomes through the PI3K pathway, microtubules, RhoA signaling, and activity of sodium-proton exchangers (NHEs) [49]. Moreover, EGF through its receptor EGFR has been shown to induce anterograde lysosomes trafficking through p38 MAPK activity and NHEs [52]. Our study identifies a new signaling cascade involving the AXL RTK, AKT/NF-κB signaling pathway and the lactate transporter MCT-1, promoting the peripheral redistribution of lysosomes and subsequent cell invasion. Interestingly, although these RTKs have overlapping downstream signaling pathways, they seem to act through distinct signaling effectors to induce peripheral distribution of lysosomes and cell invasion. EGFR- and MET-induced lysosome anterograde trafficking depends on NHEs in prostate cancer cells ([49],[52]). Although NHE-mediated proton reflux contributes to the acidification of the extracellular environment, expression of NHE1 does not appear to be regulated by AXL in our EAC cell models (data not shown). Our data show that AXL contributes to the extracellular acidification through the regulation of lactate transport.

How AXL-dependent increased extracellular acidity regulates lysosome trafficking remains to be investigated. We propose that an acidic tumor microenvironment could induce cell invasion through formation of invadopodia, which are actin-rich protrusions of the plasma membrane that are associated with degradation of the ECM in invasive cancer cells through local deposition of proteases. Future studies will be necessary to examine whether AXL-dependent extracellular acidification induces invadopodia formation and whether peripheral lysosomes localize to these protrusions resulting in cathepsin secretion and localized invasion. In support of this hypothesis, it has been shown that LAMP1-positive vesicles are present in invadopodia [58]. Moreover, invadopodia have been shown to be critical docking and secretion sites for multivesicular endosomes, which fuse with the plasma membrane for exosome secretion [59].

Conclusions

In summary, we addressed the role of AXL in cell invasion by proposing a novel mechanism that implicates upregulation of extracellular acidification, lysosomes peripheral distribution, and exocytosis. Targeting AXL with the specific tyrosine kinase inhibitor R428 (BGB324) reverses these effects and effectively reduces cell invasion. Given our current knowledge of the mechanistic role of AXL in regulating cancer cell invasion, our data support future clinical trials to evaluate the therapeutic potential of R428 in highly invasive EAC.

Supplementary data to this article can be found online at https://doi.org/10.1016/j.neo.2018.08.005.

References

[1] Napier KJ, Scheerer M, and Misra S (2014). Esophageal cancer: a review of epidemiology, pathogenesis, staging workup and treatment modalities. *World J Gastrointest Oncol* **6**, 112–120.

[2] Coleman HG, Xie S-H, and Lagergren J (2018). The epidemiology of esophageal adenocarcinoma. *Gastroenterology* **154**, 390–405.

[3] Hur C, Miller M, Kong CY, Dowling EC, Nattinger KJ, Dunn M, and Feuer EJ (2013). Trends in esophageal adenocarcinoma incidence and mortality. *Cancer* **119**, 1149–1158.

[4] Lagergren J and Lagergren P (2013). Recent developments in esophageal adenocarcinoma. *CA Cancer J Clin* **63**, 232–248.

[5] Rubenstein JH and Shaheen NJ (2015). Epidemiology, diagnosis, and management of esophageal adenocarcinoma. *Gastroenterology* **149**, 302–317.e1.

[6] O'Bryan JP, Frye RA, Cogswell PC, Neubauer A, Kitch B, Prokop C, Espinosa R, Le Beau MM, Earp HS, and Liu ET (1991). axl, a transforming gene isolated from primary human myeloid leukemia cells, encodes a novel receptor tyrosine kinase. *Mol Cell Biol* **11**, 5016–5031.

[7] Hector A, Montgomery EA, Karikari C, Canto M, Dunbar KB, Wang JS, Feldmann G, Hong S-M, Haffner MC, and Meeker AK, et al (2010). The Axl receptor tyrosine kinase is an adverse prognostic factor and a therapeutic target in esophageal adenocarcinoma. *Cancer Biol Ther* **10**, 1009–1018.

[8] Fridell YW, Jin Y, Quilliam LA, Burchert A, McCloskey P, Spizz G, Varnum B, Der C, and Liu ET (1996). Differential activation of the Ras/extracellular-signal-regulated protein kinase pathway is responsible for the biological consequences induced by the Axl receptor tyrosine kinase. *Mol Cell Biol* **16**, 135–145.

[9] Gjerdrum C, Tiron C, Høiby T, Stefansson I, Haugen H, Sandal T, Collett K, Li S, McCormack E, and Gjertsen BT, et al (2010). Axl is an essential epithelial-to-mesenchymal transition-induced regulator of breast cancer metastasis and patient survival. *Proc Natl Acad Sci U S A* **107**, 1124–1129.

[10] Goruppi S, Ruaro E, Varnum B, and Schneider C (1997). Requirement of phosphatidylinositol 3-kinase-dependent pathway and Src for Gas6-Axl mitogenic and survival activities in NIH 3T3 fibroblasts. *Mol Cell Biol* **17**, 4442–4453.

[11] Li Y, Ye X, Tan C, Hongo J-A, Zha J, Liu J, Kallop D, Ludlam MJC, and Pei L (2009). Axl as a potential therapeutic target in cancer: role of Axl in tumor growth, metastasis and angiogenesis. *Oncogene* **28**, 3442–3455.

[12] Hämälistö S and Jäättelä M (2016). Lysosomes in cancer-living on the edge (of the cell). *Curr Opin Cell Biol* **39**, 69–76.

[13] Kallunki T, Olsen OD, and Jäättelä M (2013). Cancer-associated lysosomal changes: friends or foes? *Oncogene* **32**, 1995–2004.

[14] Machado E, White-Gilbertson S, van de Vlekkert D, Janke L, Moshiach S, Campos Y, Finkelstein D, Gomero E, Mosca R, and Qiu X, et al (2015). Regulated lysosomal exocytosis mediates cancer progression. *Sci Adv* **1**e1500603.

[15] Olson OC and Joyce JA (2015). Cysteine cathepsin proteases: regulators of cancer progression and therapeutic response. *Nat Rev Cancer* **15**, 712–729.

[16] Yogalingam G, Bonten EJ, van de Vlekkert D, Hu H, Moshiach S, Connell SA, and d'Azzo A (2008). Neuraminidase 1 is a negative regulator of lysosomal exocytosis. *Dev Cell* **15**, 74–86.

[17] Chen S, Dong H, Yang S, and Guo H (2017). Cathepsins in digestive cancers. *Oncotarget* **8**, 41690–41700.

[18] Aggarwal N and Sloane BF (2014). Cathepsin B: multiple roles in cancer. *Proteomics Clin Appl* **8**, 427–437.

[19] Sameni M, Elliott E, Ziegler G, Fortgens PH, Dennison C, and Sloane BF (1995). Cathepsin B and D are localized at the surface of human breast cancer cells. *Pathol Oncol Res* **1**, 43–53.

[20] Warburg O, Wind F, and Negelein E (1927). The metabolism of tumors in the body. *J Gen Physiol* **8**, 519–530.

[21] McFate T, Mohyeldin A, Lu H, Thakar J, Henriques J, Halim ND, Wu H, Schell MJ, Tsang TM, and Teahan O, et al (2008). Pyruvate dehydrogenase complex activity controls metabolic and malignant phenotype in cancer cells. *J Biol Chem* **283**, 22700–22708.

[22] Walenta S, Salameh A, Lyng H, Evensen JF, Mitze M, Rofstad EK, and Mueller-Klieser W (1997). Correlation of high lactate levels in head and neck tumors with incidence of metastasis. *Am J Pathol* **150**, 409–415.

[23] Estrella V, Chen T, Lloyd M, Wojtkowiak J, Cornnell HH, Ibrahim-Hashim A, Bailey K, Balagurunathan Y, Rothberg JM, and Sloane BF, et al (2013). Acidity generated by the tumor microenvironment drives local invasion. *Cancer Res* **73**, 1524–1535.

[24] Kato Y, Ozawa S, Miyamoto C, Maehata Y, Suzuki A, Maeda T, and Baba Y (2013). Acidic extracellular microenvironment and cancer. *Cancer Cell Int* **13**, 89–96.

[25] Damaghi M, Tafreshi NK, Lloyd MC, Sprung R, Estrella V, Wojtkowiak JW, Morse DL, Koomen JM, Bui MM, and Gatenby RA, et al (2015). Chronic acidosis in the tumour microenvironment selects for overexpression of LAMP2 in the plasma membrane. *Nat Commun* **6**, 8752–8764.

[26] Halestrap AP and Wilson MC (2012). The monocarboxylate transporter family—role and regulation. *IUBMB Life* **64**, 109–119.

[27] Le Floch R, Chiche J, Marchiq I, Naiken T, Naïken T, Ilc K, Ilk K, Murray CM, Critchlow SE, and Roux D, et al (2011). CD147 subunit of lactate/H+ symporters MCT1 and hypoxia-inducible MCT4 is critical for energetics and growth of glycolytic tumors. *Proc Natl Acad Sci U S A* **108**, 16663–16668.

[28] Morais-Santos F, Granja S, Miranda-Gonçalves V, Moreira AHJ, Queirós S, Vilaça JL, Schmitt FC, Longatto-Filho A, Paredes J, and Baltazar F, et al (2015). Targeting lactate transport suppresses in vivo breast tumour growth. *Oncotarget* **6**, 19177–19189.

[29] De Saedeleer CJ, Porporato PE, Copetti T, Pérez-Escuredo J, Payen VL, Brisson L, Feron O, and Sonveaux P (2014). Glucose deprivation increases monocarboxylate transporter 1 (MCT1) expression and MCT1-dependent tumor cell migration. *Oncogene* **33**, 4060–4068.

[30] Izumi H, Takahashi M, Uramoto H, Nakayama Y, Oyama T, Wang K-Y, Sasaguri Y, Nishizawa S, and Kohno K (2011). Monocarboxylate transporters 1 and 4 are involved in the invasion activity of human lung cancer cells. *Cancer Sci* **102**, 1007–1013.

[31] Kong SC, Nøhr-Nielsen A, Zeeberg K, Reshkin SJ, Hoffmann EK, Novak I, and Pedersen SF (2016). Monocarboxylate transporters MCT1 and MCT4 regulate migration and invasion of pancreatic ductal adenocarcinoma cells. *Pancreas* **45**, 1036–1047.

[32] Boidot R, Végran F, Meulle A, Le Breton A, Dessy C, Sonveaux P, Lizard-Nacol S, and Feron O (2012). Regulation of monocarboxylate transporter MCT1 expression by p53 mediates inward and outward lactate fluxes in tumors. *Cancer Res* **72**, 939–948.

[33] Cuff MA and Shirazi-Beechey SP (2002). The human monocarboxylate transporter, MCT1: genomic organization and promoter analysis. *Biochem Biophys Res Commun* **292**, 1048–1056.

[34] Paccez JD, Duncan K, Vava A, Correa RG, Libermann TA, Parker MI, and Zerbini LF (2015). Inactivation of GSK3β and activation of NF-κB pathway via Axl represents an important mediator of tumorigenesis in esophageal squamous cell carcinoma. *Mol Biol Cell* **26**, 821–831.

[35] Deryugina EI and Quigley JP (2008). Chick embryo chorioallantoic membrane model systems to study and visualize human tumor cell metastasis. *Histochem Cell Biol* **130**, 1119–1130.

[36] Boerboom RA, Krahn KN, Megens RTA, van Zandvoort MAMJ, Merkx M, and Bouten CVC (2007). High resolution imaging of collagen organisation and synthesis using a versatile collagen specific probe. *J Struct Biol* **159**, 392–399.

[37] Krahn KN, Bouten CVC, van Tuijl S, van Zandvoort MAMJ, and Merkx M (2006). Fluorescently labeled collagen binding proteins allow specific visualization of collagen in tissues and live cell culture. *Anal Biochem* **350**, 177–185.

[38] Demetteo RP, Heinrich MC, El-Rifai WM, and Demetri G (2002). Clinical management of gastrointestinal stromal tumors: before and after STI-571. *Hum Pathol* **33**, 466–477.

[39] Voon DC, Huang RY, Jackson RA, and Thiery JP (2017). The EMT spectrum and therapeutic opportunities. *Mol Oncol* **11**, 878–891.

[40] Nabavi N, Urukova Y, Cardelli M, Aubin JE, and Harrison RE (2008). Lysosome dispersion in osteoblasts accommodates enhanced collagen production during differentiation. *J Biol Chem* **283**, 19678–19690.

[41] Dykes SS, Gray AL, Coleman DT, Saxena M, Stephens CA, Carroll JL, Pruitt K, and Cardelli JA (2016). The Arf-like GTPase Arl8b is essential for three-dimensional invasive growth of prostate cancer in vitro and xenograft formation and growth in vivo. *Oncotarget* **7**, 31037–31052.

[42] Garg S, Sharma M, Ung C, Tuli A, Barral DC, Hava DL, Veerapen N, Besra GS, Hacohen N, and Brenner MB (2011). Lysosomal trafficking, antigen presentation, and microbial killing are controlled by the Arf-like GTPase Arl8b. *Immunity* **35**, 182–193.

[43] Korolchuk VI, Saiki S, Lichtenberg M, Siddiqi FH, Roberts EA, Imarisio S, Jahreiss L, Sarkar S, Futter M, and Menzies FM, et al (2011). Lysosomal positioning coordinates cellular nutrient responses. *Nat Cell Biol* **13**, 453–460.

[44] Circu ML, Dykes SS, Carroll J, Kelly K, Galiano F, Greer A, Cardelli J, and El-Osta H (2016). A novel high content imaging-based screen identifies the anti-helminthic niclosamide as an inhibitor of lysosome anterograde trafficking and prostate cancer cell invasion. *PLoS One* **11**e0146931.

[45] Andl CD, McCowan KM, Allison GL, and Rustgi AK (2010). Cathepsin B is the driving force of esophageal cell invasion in a fibroblast-dependent manner. *Neoplasia* **12**, 485–498.

[46] Gao L, Fang Y-Q, Zhang T-Y, Ge B, Tang R-J, Huang J-F, Jiang L-M, and Tan N (2015). Acidic extracellular microenvironment promotes the invasion and cathepsin B secretion of PC-3 cells. *Int J Clin Exp Med* **8**, 7367–7373.

[47] Montaser M, Lalmanach G, and Mach L (2002). CA-074, but not its methyl ester CA-074Me, is a selective inhibitor of cathepsin B within living cells. *Biol Chem* **383**, 1305–1308.

[48] Glunde K, Guggino SE, Solaiyappan M, Pathak AP, Ichikawa Y, and Bhujwalla ZM (2003). Extracellular acidification alters lysosomal trafficking in human breast cancer cells. *Neoplasia* **5**, 533–545.

[49] Steffan JJ, Snider JL, Skalli O, Welbourne T, and Cardelli JA (2009). Na+/H+ exchangers and RhoA regulate acidic extracellular pH-induced lysosome trafficking in prostate cancer cells. *Traffic* **10**, 737–753.

[50] Borthakur A, Saksena S, Gill RK, Alrefai WA, Ramaswamy K, and Dudeja PK (2008). Regulation of monocarboxylate transporter 1 (MCT1) promoter by butyrate in human intestinal epithelial cells: involvement of NF-κB pathway. *J Cell Biochem* **103**, 1452–1463.

[51] Vuoriluoto K, Haugen H, Kiviluoto S, Mpindi J-P, Nevo J, Gjerdrum C, Tiron C, Lorens JB, and Ivaska J (2011). Vimentin regulates EMT induction by Slug and oncogenic H-Ras and migration by governing Axl expression in breast cancer. *Oncogene* **30**, 1436–1448.

[52] Dykes SS, Gao C, Songock WK, Bigelow RL, Woude GV, Bodily JM, and Cardelli JA (2017). Zinc finger E-box binding homeobox-1 (Zeb1) drives anterograde lysosome trafficking and tumor cell invasion via upregulation of Na +/H+ Exchanger-1 (NHE1). *Mol Carcinog* **56**, 722–734.

[53] Roshy S, Sloane BF, and Moin K (2003). Pericellular cathepsin B and malignant progression. *Cancer Metastasis Rev* **22**, 271–286.

[54] Bian B, Mongrain S, Cagnol S, Langlois M, Boulanger J, Bernatchez G, Carrier JC, Boudreau F, and Rivard N (2016). Cathepsin B promotes colorectal tumorigenesis, cell invasion, and metastasis. *Mol Carcinog* **55**, 671–687.

[55] Brix K, Dunkhorst A, Mayer K, and Jordans S (2008). Cysteine cathepsins: cellular roadmap to different functions. *Biochimie* **90**, 194–207.

[56] Sevenich L and Joyce JA (2014). Pericellular proteolysis in cancer. *Genes Dev* **28**, 2331–2347.

[57] Yamagata M, Hasuda K, Stamato T, and Tannock IF (1998). The contribution of lactic acid to acidification of tumours: studies of variant cells lacking lactate dehydrogenase. *Br J Cancer* **77**, 1726–1731.

[58] Tu C, Ortega-Cava CF, Chen G, Fernandes ND, Cavallo-Medved D, Sloane BF, Band V, and Band H (2008). Lysosomal cathepsin B participates in the podosome-mediated extracellular matrix degradation and invasion via secreted lysosomes in v-Src fibroblasts. *Cancer Res* **68**, 9147–9156.

[59] Hoshino D, Kirkbride KC, Costello K, Clark ES, Sinha S, Grega-Larson N, Tyska MJ, and Weaver AM (2013). Exosome secretion is enhanced by invadopodia and drives invasive behavior. *Cell Rep* **5**, 1159–1168.